Journal of Materials Chemistry C

Doping Y2O3 with Mn4+ for Energy-Efficient Lighting

Journal:	*Journal of Materials Chemistry C*
Manuscript ID	TC-ART-03-2018-001154
Article Type:	Paper
Date Submitted by the Author:	08-Mar-2018
Complete List of Authors:	Ming, Wenmei; Oak Ridge National Laboratory, Materials Science and Technology Divison Shi, Hongliang; Beihang University Du, Mao Hua ; Oak Ridge National Laboratory,

Doping Y_2O_3 with Mn^{4+} for Energy-Efficient Lighting

Wenmei Ming[1], Hongliang Shi[1,2], and Mao-Hua Du[1*]

[1]*Materials Science and Technology Division, Oak Ridge National Laboratory, Oak Ridge, TN 37831, USA*

[2]*Department of Physics, Key Laboratory of Micro-Nano Measurement-Manipulation and Physics (Ministry of Education), Beihang University, Beijing 100191, China*

*Corresponding author: Mao-Hua Du (mhdu@ornl.gov)

ABSTRACT: Developing energy-efficient LEDs that emit warm white light requires new red phosphors with appropriate emission wavelengths and band widths. Mn^{4+}-activated Y_2O_3 is a potential red LED phosphor with narrow emission and improved emission wavelength compared to previously known Mn^{4+}-activated oxide phosphors. In this work, the dopability and the oxidation state of Mn in Y_2O_3 are investigated based on formation energies of native defects, Mn dopants, and divalent co-dopants (i.e., Ca, Sr, Cd, Zn) calculated using hybrid density functional theory. We found that Mn^{4+} is difficult to form in Y_2O_3 without co-doping. Stabilizing Mn^{4+} on Y^{3+} sites (forming Mn_Y^+ donors) requires the co-doping of compensating acceptors (Ca or Sr) under oxygen-rich growth environments.

I. INTRODUCTION

White light-emitting diodes (wLEDs) are projected to play a dominant role in the future energy-efficient lighting technologies.[1-7] Although white light can be produced by combining blue, green, and red LEDs, commonly used LED lamps are mostly based on phosphor-converted

LEDs (pc-LEDs) for the ease of fabrication. For example, the most popular method of making wLEDs involves coating the InGaN blue LED with a yellow phosphor $Y_3Al_5O_{12}:Ce^{3+}$ ($YAG:Ce^{3+}$)[1-2] such that the blue emission of the InGaN LED is combined with the broad-band yellow emission of $YAG:Ce^{3+}$ to produce white light. A major drawback of such LED lamp is the lack of sufficient red component in the emission spectrum, resulting in low color rendering quality [color rendering index (CRI) usually < 80].[1-2] (The CRI measures how a light source renders the colors of objects in comparison to the standardized daylight or a black body. A CRI > 80 is usually required for indoor lighting, for which warm white light is preferred.)

The warm white light can be produced by adding a red phosphor into the phosphor blend of a blue LED. The red phosphor should absorb strongly the InGaN emission (~450 nm) and ideally should have a narrow emission band centered near 610 nm, which matches the peak human eye sensitivity to red light. Several nitride red phosphors [$(Ba,Sr)_2Si_2N_8:Eu^{2+}$ and $(Ca,Sr)SiAlN_3:Eu^{2+}$] have been shown to improve the CRI of wLEDs and have been commercialized.[8-9] However, the broad-band emission of these nitride phosphors [full width at half maxima ~90 nm] limits the luminous efficacy because a significant portion of the emission spectra is deep red, to which the human eyes are not sufficiently sensitive.

Mn^{4+}-doped fluorides and oxides are a large class of red- and deep-red-emitting phosphors with line-shaped narrow emission.[10-13] Several Mn^{4+}-doped fluorides exhibit favorable optical properties for LED lighting. For example, $K_2SiF_6:Mn^{4+}$ can be excited at 450 nm and has narrow emission centered near 630 nm.[10, 13] However, Mn^{4+} activated fluoride phosphors have the problem of hygroscopicity, which limits their applications.[2] Oxides are chemically more stable but Mn^{4+} emission wavelengths in oxides are usually > 650 nm,[11] resulting in unsatisfactory luminous efficacy. Currently, the shortest reported Mn^{4+} emission wavelength in oxides is 648 nm for $Y_2Sn_2O_7$.[11] Therefore, developing Mn^{4+} activated red-emitting oxide phosphors with emitting wavelength closer to 610 nm is urgently needed.

Recent theoretical studies show that the Mn^{4+} emission wavelength strongly depends on the hybridization between the Mn^{4+} ion and its ligands.[11-12] Weaker hybridization generally leads to shorter emission wavelength, which explains the observed shorter emission wavelength in fluorides than in oxides. The Mn^{4+} ion is typically octahedrally coordinated because the Mn^{4+} ion is a d^3 ion, which can be stabilized by the octahedral crystal field.[12] Density functional theory (DFT) calculations showed that longer Mn-ligand bond lengths and stronger bond angle distortion in the octahedral structure lead to weaker Mn-ligand hybridization, which reduces the emission wavelength.[12] Several Mn^{4+} activated oxides have been proposed to have shorter emission wavelengths than 650 nm based on DFT calculations. Among them, Y_2O_3:Mn^{4+} was predicted to have the shortest emission wavelength.[12]

The Mn ion is multivalent with several possible oxidation states (such as 2+, 3+, and 4+). Stabilizing the 4+ oxidation state of Mn at high doping level may be challenging because Mn^{4+} is an electron donor in Y_2O_3. Broad-band yellow emission from Mn^{2+} dopants in Y_2O_3 has been observed[14] but the line-shaped narrow red emission of Mn^{4+} has not been reported, indicating that stabilizing Mn^{4+} as an electron donor in Y_2O_3 may be challenging. In this paper, we show hybrid density functional calculations of native defects, Mn dopants, and divalent metal co-dopants (Ca, Sr, Cd, Zn) in Y_2O_3. The results show that co-doping Y_2O_3 by compensating acceptors (Ca or Sr) and applying oxygen overpressure can stabilize Mn^{4+} in Y_2O_3.

II. Computational Methods

Our calculations are based on density functional theory (DFT) implemented in the plane-wave basis VASP code.[15] The projector augmented wave method was used to describe the interaction between ions and electrons.[16] The kinetic energy cutoff is 400 eV. The reciprocal-space integrations were performed on a 2 ×2×2 k-point mesh. Heyd-Scuseria-Ernzerhof (HSE) hybrid functional [17-18] (which includes 25% Hartree-Fock exchange) was adopted for all calculations. Experimental lattice constants[19] of cubic bixbyite Y_2O_3 (space group 206, Ia3) were used: a = b = c = 10.6038 Å. The atomic positions were relaxed until the residual forces were less than 0.05 eV/Å. The calculated band gap is 5.7 eV, in excellent agreement with the experimental band gap of 5.8 eV.[20]

The defect (or dopant) formation energy **V***H* was calculated using[21]

$$\mathrm{V}H = (E_D - E_0) - \sum_i n_i(\mu_i + \mu_i^{ref}) + q(\varepsilon_{VBM} + \varepsilon_f) + \mathrm{V}E_{corr} \quad . \tag{1}$$

Here, E_D and E_0 in the first term are the total energies of the defect-containing and the defect-free cells. The second term in Eq. (1) is the change in energy due to the exchange of atoms with their reservoirs. n_i is the difference in the number of atoms for the *i*th atomic species between the defect-containing and defect-free supercells. μ_i is the chemical potential of the *i*th atomic species relative to its reference chemical potential μ_i^{ref}. For Y, μ_i^{ref} is chosen as the chemical potential of Y in bulk Y; for oxygen, μ_i^{ref} is taken as half of the energy of an isolated O_2 molecule. The third term is the change in energy due to the exchange of electrons with their reservoir. q is the defect charge state. ε_{VBM} is the energy of the valence band maximum (VBM) of Y_2O_3. ε_f is the Fermi energy relative to the VBM and can be varied between the VBM and the conduction band minimum (CBM). The fourth term includes potential alignment and image charge corrections.[22]

The chemical potentials in Eq. 1 are subject to constraints under thermal equilibrium. To maintain the stability of Y_2O_3 during growth, the chemical potentials of Y and O should satisfy the following:

$$2\mu_{\mathrm{Y}} + 3\mu_{\mathrm{O}} = \Delta H(\mathrm{Y_2O_3}) \tag{2}$$

$$\mu_{\mathrm{Y}} \le 0,\ \mu_{\mathrm{O}} \le 0 \tag{3}$$

$\Delta H(\mathrm{Y_2O_3})$ is the enthalpy of formation for Y_2O_3. In the case of Mn doping, the Mn chemical potential, μ_{Mn}, has the following constraints, which are applied to avoid the formation of unwanted elemental Mn and Mn-oxide phases:

$$\begin{gathered}
\mu_{\mathrm{Mn}} \le 0 \\
\mu_{\mathrm{Mn}} + \mu_{\mathrm{O}} \le \Delta H(\mathrm{MnO}) \\
\mu_{\mathrm{Mn}} + 2\mu_{\mathrm{O}} \le \Delta H(\mathrm{MnO_2}) \\
2\mu_{\mathrm{Mn}} + 3\mu_{\mathrm{O}} \le \Delta H(\mathrm{Mn_2O_3}) \\
3\mu_{\mathrm{Mn}} + 4\mu_{\mathrm{O}} \le \Delta H(\mathrm{Mn_3O_4}) \\
5\mu_{\mathrm{Mn}} + 8\mu_{\mathrm{O}} \le \Delta H(\mathrm{Mn_5O_8}) \\
2\mu_{\mathrm{Y}} + 2\mu_{\mathrm{Mn}} + 7\mu_{\mathrm{O}} \le \Delta H(\mathrm{Y_2Mn_2O_7}) \\
\mu_{\mathrm{Y}} + \mu_{\mathrm{Mn}} + 3\mu_{\mathrm{O}} \le \Delta H(\mathrm{YMnO_3}) \\
\mu_{\mathrm{Y}} + 2\mu_{\mathrm{Mn}} + 5\mu_{\mathrm{O}} \le \Delta H(\mathrm{YMn_2O_5})
\end{gathered} \tag{4}$$

Here, $\Delta H(\mathrm{MnO})$, $\Delta H(\mathrm{MnO_2})$, $\Delta H(\mathrm{Mn_2O_3})$, $\Delta H(\mathrm{Mn_3O_4})$, $\Delta H(\mathrm{Mn_5O_8})$, $\Delta H(\mathrm{Y_2Mn_2O_7})$, $\Delta H(\mathrm{YMnO_3})$, and $\Delta H(\mathrm{YMn_2O_5})$ are the enthalpies of formation for MnO, MnO_2, Mn_2O_3, Mn_3O_4, Mn_5O_8, $Y_2Mn_2O_7$, $YMnO_3$, and YMn_2O_5, respectively.

We have also investigated doping by divalent cations (i.e., Ca, Sr, Zn, Cd). The chemical potentials of these dopants are constrained to prevent the formation of metal and metal-oxide secondary phases:

$$\mu_{\mathrm{Ca}} \le 0,\ \mu_{\mathrm{Sr}} \le 0,\ \mu_{\mathrm{Cd}} \le 0,\ \mu_{\mathrm{Zn}} \le 0$$

$$\begin{aligned} &\mu_{\mathrm{Ca}} + \mu_{\mathrm{O}} \le \Delta H(\mathrm{CaO}) \\ &\mu_{\mathrm{Sr}} + \mu_{\mathrm{O}} \le \Delta H(\mathrm{SrO}) \\ &\mu_{\mathrm{Cd}} + \mu_{\mathrm{O}} \le \Delta H(\mathrm{CdO}) \\ &\mu_{\mathrm{Zn}} + \mu_{\mathrm{O}} \le \Delta H(\mathrm{ZnO}) \end{aligned} \tag{5}$$

Here, $\Delta H(\mathrm{CaO})$, $\Delta H(\mathrm{Sr\,O})$, $\Delta H(\mathrm{CdO})$, and $\Delta H(\mathrm{ZnO})$ are the enthalpies of formation for CaO, SrO, CdO, and ZnO, respectively.

III. Results and Discussion

The crystal structure Y_2O_3 as shown in Figure 1 can be viewed as the fluorite CaF_2 structure[23] with 1/4 of the oxygen atoms removed. All the O sites are equivalent (48e site). The Y ions have two inequivalent sites, 8b and 24d. The 8b site has six O nearest neighbors in a distorted octahedral environment, which can stabilize Mn^{4+}.[12] Indeed, the Mn^{4+} ion on the 8b site is more stable than that on the 24d site by 0.47 eV based on HSE calculations. Figure 2 shows the formation energies of vacancy and interstitial defects as well as substitutional and interstitial Mn dopants at both O-poor and O-rich limits. The maximal Mn chemical potential that satisfies Eq. (4) was used in calculations. It can be seen in Fig. 2 that the most important native donor and acceptor defects are the oxygen vacancy (V_{O}) and the oxygen interstitial (O_i). The substitutional $\mathrm{Mn_Y}$ can take three different charge states (+1, 0, and -1) depending on the Fermi level. $\mathrm{Mn_Y^+}$ (in which a Y^{3+} ion is substituted by a Mn^{4+} ion) is most stable in p-type Y_2O_3 where the Fermi level is low. Under the O-rich condition [Fig. 2(b)], or equivalently the Y-poor condition, Mn_Y^+ is the dominant electron donor (more abundant than V_O and Mn_i) in Y_2O_3.

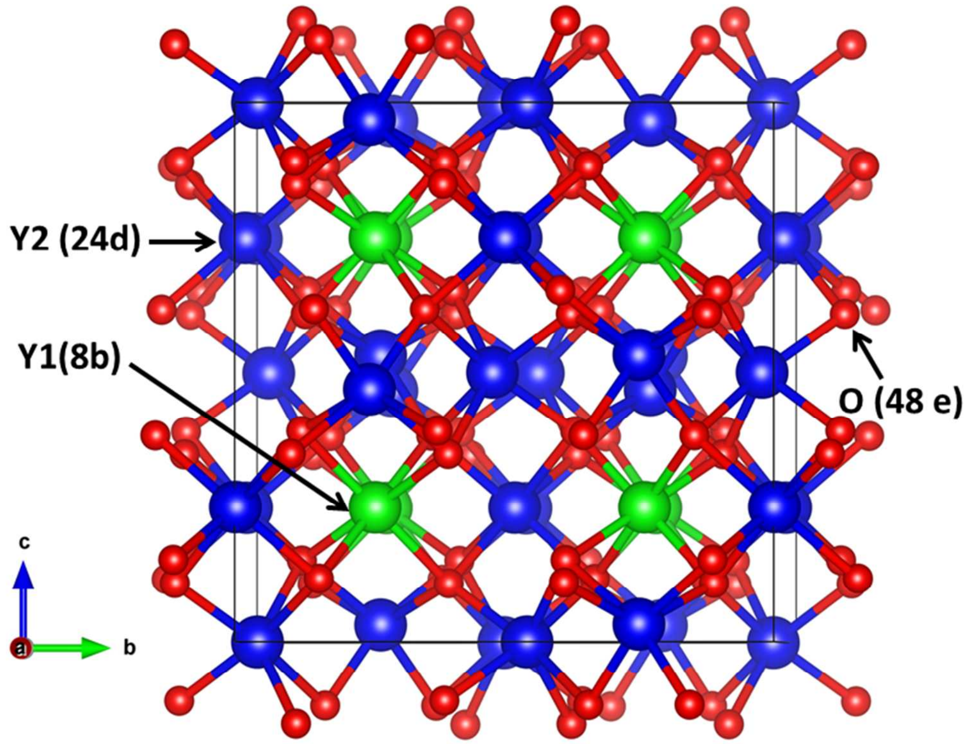

Figure 1. Crystal structure of bixbyite cubic Y_2O_3. The yttrium cations on the 24d and the 8b sites are represented by the blue and the green balls, respectively, while the oxygen anions are represented by the red balls.

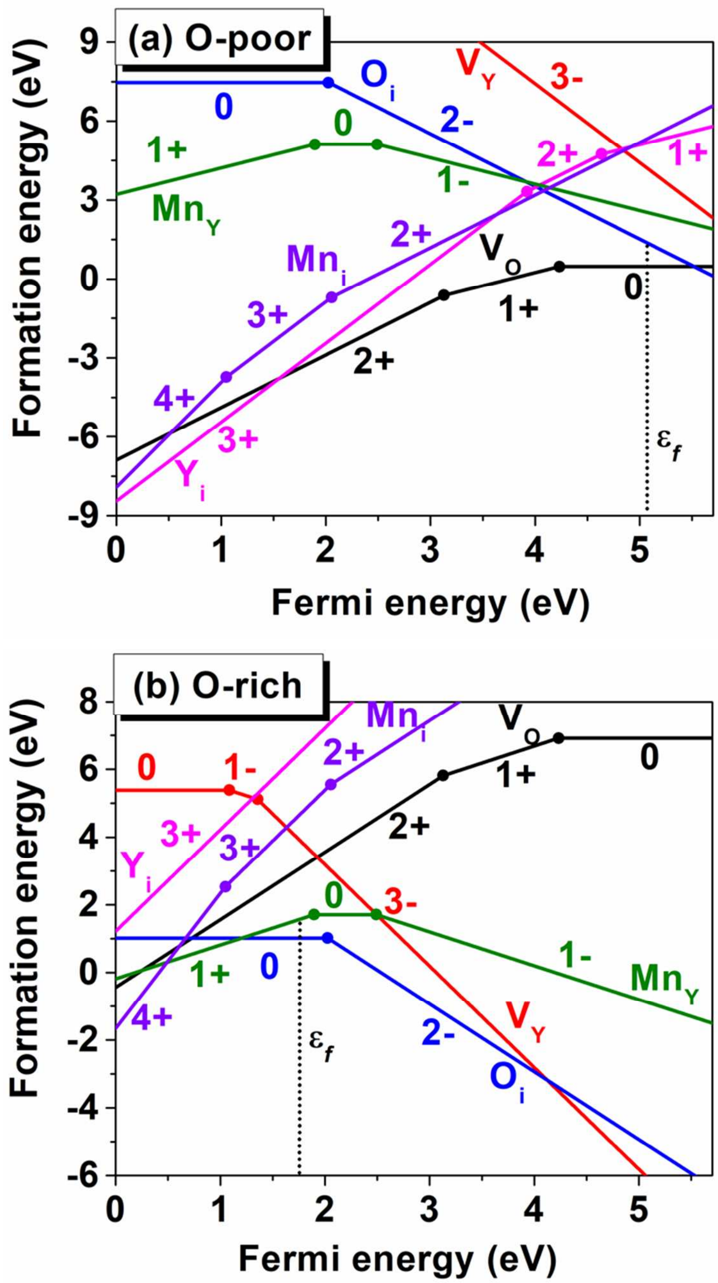

Figure 2. Formation energies of native defects and Mn dopants in Y_2O_3 at (a) the O-poor and (b) the O-rich limits. The maximally allowed Mn chemical potential is used. The slope of the formation-energy line indicates the charge state of the defect/dopant. The dotted lines indicate the Fermi level (ε_f), which is pinned approximately by the formation-energy lines of the lowest-energy donor and acceptor.

The Fermi level in Y_2O_3 is pinned approximately at the point where the formation-energy lines of the lowest-energy donor and acceptor intersect. If the Fermi level is deep inside the band gap, the free carrier density is negligible, and the donor density is nearly equal to the acceptor density; therefore, the charge neutrality condition is satisfied. At the O-poor limit [Figure 2(a)], the Fermi level is pinned by V_O^+ and O_i^{2-} within the n-type region, favoring Mn_Y^-. At the O-rich limit [Figure 2(b)], the Fermi level is pinned by Mn_Y^+ and O_i^{2-}, slightly below the (+/0) transition level of Mn_Y; thus, Mn_Y^+ is the most stable. The results in Figure 2 show that the highly O-rich growth environment is needed to stabilize Mn_Y^+ in Y_2O_3.

Next, we investigate the effect of acceptor doping on the Fermi level and the oxidation state of Mn_Y in Y_2O_3. The formation energies of substitutional and interstitial divalent cations Ca, Sr, Cd, and Zn were calculated at the O rich limit, at which the formation of Mn_Y is most favored (Figure 3). The maximal chemical potentials of Ca, Sr, Cd, and Zn that satisfy Eq. 5 were used. The substitutional Ca_Y, Sr_Y, Cd_Y, and Zn_Y are acceptors while the interstitial Ca_i, Sr_i, Cd_i, and Zn_i are donors. These donors have high formation energies and are thus not important for charge compensation. Among the above acceptor dopants, Ca_Y^-, Sr_Y^-, and Cd_Y^- have relatively low formation energies; thus, the Fermi level is pinned by the acceptor dopant and the Mn_Y^+ donor as shown in Figures 3(a)-(c). The lower Fermi level as the result of the acceptor doping of Ca, Sr, and Cd promotes the formation of Mn_Y^+. On the other hand, Zn_Y^- has relatively high formation energy (~ 1 eV higher than those of Ca_Y^-, Sr_Y^-, and Cd_Y^-) and thus does not significantly affect the Fermi level and the concentration of Mn_Y^+. We have also investigated N doping on the O site (N_O). However, N_O have high formation energy (not shown) and thus cannot lower the Fermi level. The high formation energy of N_O is due to the high energy cost of breaking the triple bond in a N_2 molecule.

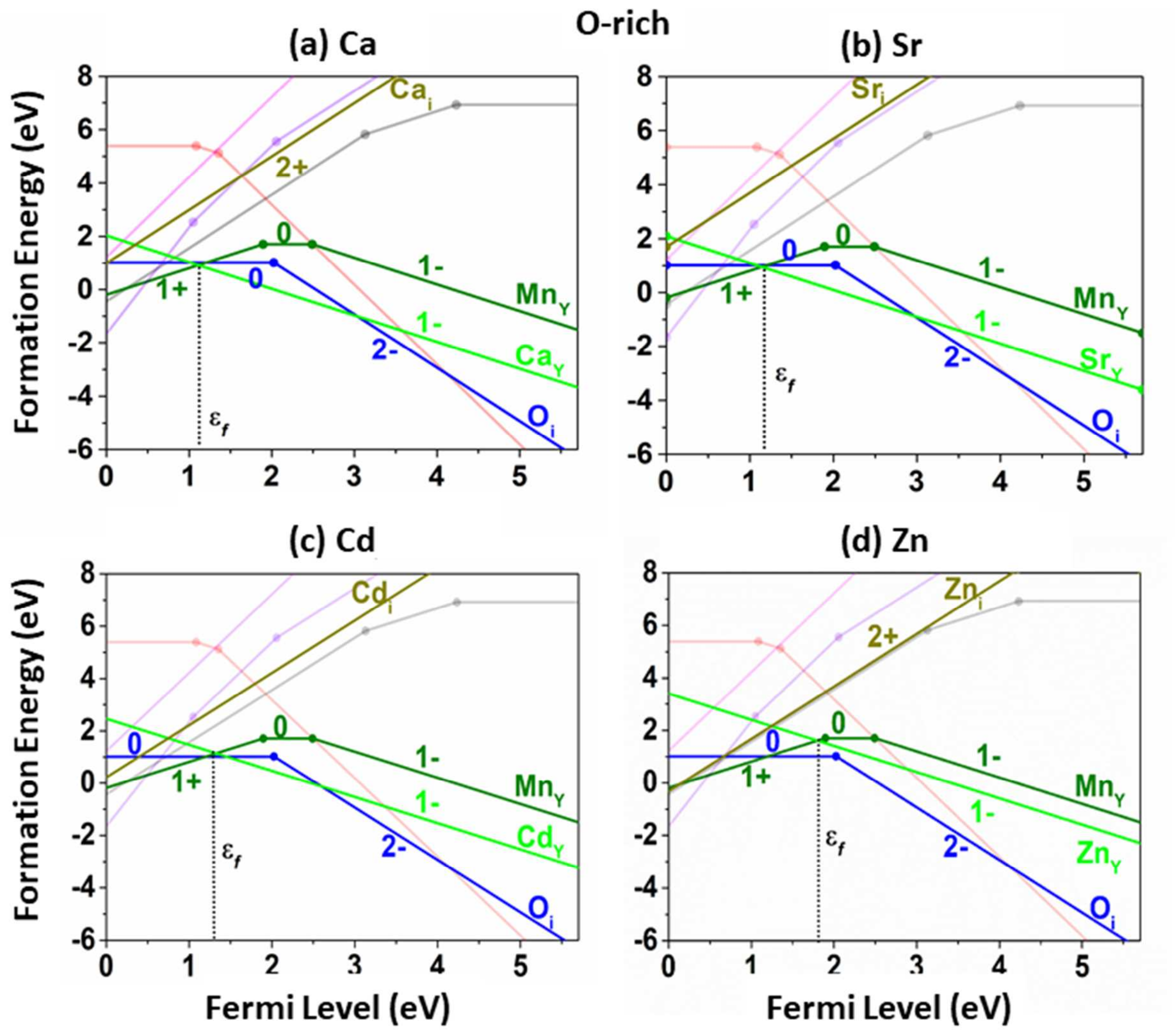

Figure 3. Formation energies of divalent dopants (a) Ca, (b) Sr, (c) Cd, and (d) Zn as well as the Mn dopant and native defects in Y_2O_3 under the O-rich limit. The maximally allowed Ca, Sr, Cd, Zn, and Mn chemical potentials are used. The dotted lines indicate the Fermi level (ε_f), which is pinned approximately by the formation energy lines of the lowest-energy donor and acceptor.

The O chemical potential used in Figure 3 is half of the total energy of an isolated O_2 molecule [$\frac{1}{2}E(O_2)$], which is the O-rich limit. However, the effect of temperature and pressure on the O chemical potential may not be neglected for the gas-phase O_2 molecules. Using the experimentally measured thermochemical table NIST-JANAF,[24] one can obtain the O chemical potential $\mu_O(T,P_0)$ at any given temperature T and the pressure P_0 = 1 atm. Note that $\mu_O(T,P_0)$ is relative to $\mu_O(0\ \mathrm{K},P_0)$, which is taken as $\frac{1}{2}E(O_2)$ from the calculation. Next, using the ideal gas law, the O chemical potential at any temperature and pressure $\mu_O(T,P)$ can be calculated by

$$\mu_O(T,P)=\mu_O(T,P_0)+\frac{1}{2}k_BT\ln(P/P_0). \qquad (6)$$ [25]

Since phosphors are usually synthesized by solid state reaction firing in air at high temperatures (T > 1000 ºC)[26], we calculated the defect and dopant formation energies under the condition P_{O_2} = 0.21 atm (the oxygen partial pressure in air) and T = 1300 K, which results in μ_O = -1.58 eV. Under this condition, μ_Y is increased compared to that at the oxygen-rich limit (μ_O = 0) due to Eq. 2, which makes removing Y cost more energy; on the other hand, the maximally allowed μ_{Mn} is also increased due to Eq. 4, which reduces the energy cost of incorporating Mn in Y_2O_3. The above two effects on the formation energy of Mn_Y partially cancel each other. The resulting formation energy of Mn_Y (in Fig. 4) is lowered compared to that at the O-rich limit (Fig. 3). Without acceptor doping, the Fermi level is pinned by Mn_Y^+ and Mn_Y^- between the (+/0) and the (0/-) levels of Mn_Y, favoring the formation of Mn_Y^0. With Ca or Sr co-doping, the Fermi level is pinned by Mn_Y^+ and the acceptor below the (+/0) transition level of Mn_Y [Figs. 4(a)-(b)], favoring Mn_Y^+ over Mn_Y^0. With the use of more realistic O chemical potential that takes into account the effects of temperature and pressure, it is determined that the acceptor doping is required for stabilization of $\mathrm{Mn_Y^+}$ (or $\mathrm{Mn^{4+}}$). Based on Eqs. (1), (2), and (5), it can be shown that the formation energy of a substitutional divalent dopant (such as Ca and Sr) at its maximally allowed chemical potential is related to the O chemical potential through $-\frac{1}{2}\mu_\mathrm{O}$. Thus, increasing the O chemical potential by increasing the O partial pressure or by lowering the temperature can further reduce the formation energy of divalent acceptor dopants, which lowers the Fermi level and increase the concentration of $\mathrm{Mn_Y^+}$.

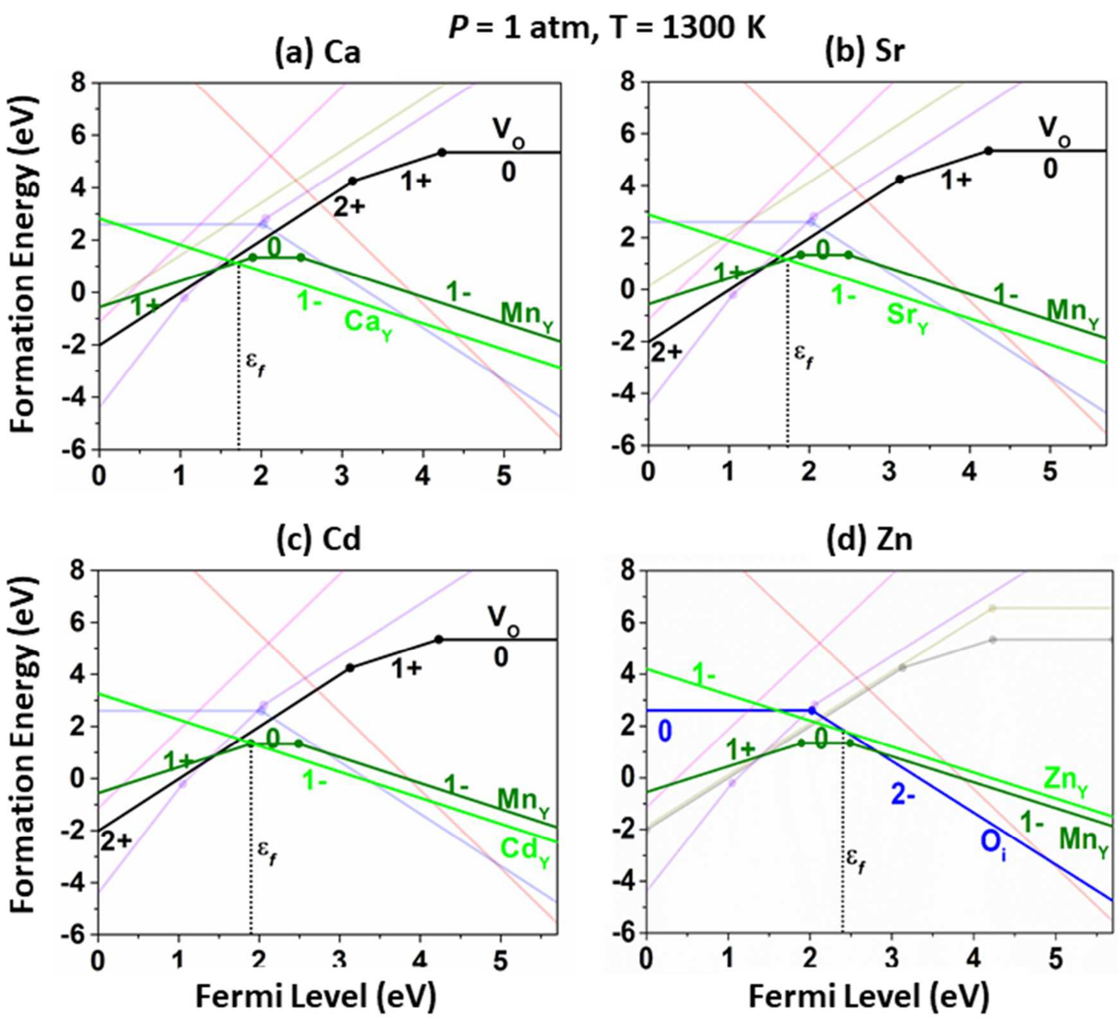

Figure 4. Formation energies of divalent dopants (a) Ca, (b) Sr, (c) Cd, and (d) Zn as well as Mn dopants and native defects in Y_2O_3 calculated under the condition of P = 1 atm (the oxygen partial pressure in air P_{O_2} = 0.21 atm) and T = 1300 K. The maximally allowed chemical potentials of Ca, Sr, Cd, Zn, and Mn are used. The dotted lines indicate the Fermi level (ε_f), which is pinned approximately by the formation-energy lines of the lowest-energy donor and acceptor.

Summary

Y_2O_3:Mn^{4+} is a potential LED red phosphor with improved emission wavelength compared to previously known Mn^{4+} activated oxides. In this work, we systematically studied the dopability of Mn^{4+} in Y_2O_3 by calculating the formation energies of native defects, Mn dopants at different oxidation states, and the co-dopants (Ca, Sr, Cd, Zn) based on hybrid density functional theory. We show that Mn^{4+} in Y_2O_3 can be stabilized by co-doping by compensating acceptors Ca and Sr. Creating an O-rich growth condition by applying oxygen overpressure should help increase the Mn^{4+} concentration in Y_2O_3. These results may motivate future experimental efforts in developing Mn^{4+} activated Y_2O_3 for LED lighting.

ACKNOWLEDGMENTS

We are grateful for the useful discussion with Alok M. Srivastava, Stephen A. Payne, Nerine J. Cherepy, Craig A. Bridges, Charles L. Melcher, and Mariya Zhuravleva. The calculations on Mn dopants in Y_2O_3 (M. H. Du) were supported by the Critical Materials Institute, an Energy Innovation Hub funded by the U.S. Department of Energy, Office of Energy Efficiency and

Renewable Energy, Advanced Manufacturing Office. The calculations on native defects in Y_2O_3 (W. Ming, H. Shi, M. H. Du) were supported by the U. S. Department of Energy, Office of Science, Basic Energy Sciences, Materials Sciences and Engineering Division. H. Shi was partially supported by the National Natural Science Foundation of China (NSFC) under Grants No.11604007 and the start-up funding at Beihang University.

1. McKittrick, J.; Shea-Rohwer, L. E., Review: Down Conversion Materials for Solid-State Lighting. *Journal of the American Ceramic Society* **2014,** *97* (5), 1327-1352.
2. Meyer, J.; Tappe, F., Photoluminescent Materials for Solid-State Lighting: State of the Art and Future Challenges. *Advanced Optical Materials* **2015,** *3* (4), 424-430.
3. Oh, J. H.; Eo, Y. J.; Yoon, H. C.; Huh, Y.-D.; Do, Y. R., Evaluation of new color metrics: guidelines for developing narrow-band red phosphors for WLEDs. *Journal of Materials Chemistry C* **2016,** *4* (36), 8326-8348.
4. Xie, R.-J.; Hirosaki, N.; Takeda, T.; Suehiro, T., On the Performance Enhancement of Nitride Phosphors as Spectral Conversion Materials in Solid State Lighting. *ECS J. Solid State Sci. Technol.* **2013,** *2* (2), R3031-R3040.
5. Li, J.; Yan, J.; Wen, D.; Khan, W. U.; Shi, J.; Wu, M.; Su, Q.; Tanner, P. A., Advanced red phosphors for white light-emitting diodes. *Journal of Materials Chemistry C* **2016,** *4* (37), 8611-8623.
6. Setlur, A. A.; Lyons, R. J.; Murphy, J. E.; Prasanth Kumar, N.; Satya Kishore, M., Blue Light-Emitting Diode Phosphors Based upon Oxide, Oxyhalide, and Halide Hosts. *ECS J. Solid State Sci. Technol.* **2013,** *2* (2), R3059-R3070.
7. McKittrick, J.; Hannah, M. E.; Piquette, A.; Han, J. K.; Choi, J. I.; Anc, M.; Galvez, M.; Lugauer, H.; Talbot, J. B.; Mishra, K. C., Phosphor Selection Considerations for Near-UV LED Solid State Lighting. *ECS J. Solid State Sci. Technol.* **2013,** *2* (2), R3119-R3131.
8. Uheda, K.; Hirosaki, N.; Yamamoto, Y.; Naito, A.; Nakajima, T.; Yamamoto, H., Luminescence Properties of a Red Phosphor, CaAlSiN3 : Eu2 + , for White Light-Emitting Diodes. *Electrochemical and Solid-State Letters* **2006,** *9* (4), H22-H25.
9. Xie, R.-J.; Hirosaki, N.; Suehiro, T.; Xu, F.-F.; Mitomo, M., A Simple, Efficient Synthetic Route to Sr2Si5N8:Eu2+-Based Red Phosphors for White Light-Emitting Diodes. *Chemistry of Materials* **2006,** *18* (23), 5578-5583.
10. Sijbom, H. F.; Verstraete, R.; Joos, J. J.; Poelman, D.; Smet, P. F., K2SiF6:Mn4+ as a red phosphor for displays and warm-white LEDs: a review of properties and perspectives. *Opt. Mater. Express* **2017,** *7* (9), 3332-3365.
11. Brik, M. G.; Srivastava, A. M., On the optical properties of the Mn4+ ion in solids. *Journal of Luminescence* **2013,** *133*, 69-72.
12. Du, M. H., Chemical trends of Mn4+ emission in solids. *Journal of Materials Chemistry C* **2014,** *2* (14), 2475-2481.
13. Takahashi, T.; Adachi, S., Mn4+-activated red photoluminescence in K2SiF6 phosphor. *Journal of The Electrochemical Society* **2008,** *155* (12), E183-E188.
14. Minami, T.; Kobayashi, Y.; Miyata, T.; Yamazaki, M., High-luminance thin-film electroluminescent devices using Y2O3:Mn phosphor. *Thin Solid Films* **2003,** *443* (1), 91-96.

15. Kresse, G.; Furthmüller, J., Efficiency of ab-initio total energy calculations for metals and semiconductors using a plane-wave basis set. *Computational Materials Science* **1996,** *6* (1), 15-50.
16. Kresse, G.; Joubert, D., From ultrasoft pseudopotentials to the projector augmented-wave method. *Physical Review B* **1999,** *59* (3), 1758.
17. Heyd, J.; Scuseria, G. E.; Ernzerhof, M., Hybrid functionals based on a screened Coulomb potential. *Journal of Chemical Physics* **2003,** *118* (18), 8207-8215.
18. Krukau, A. V.; Vydrov, O. A.; Izmaylov, A. F.; Scuseria, G. E., Influence of the exchange screening parameter on the performance of screened hybrid functionals. *Journal of Chemical Physics* **2006,** *125* (22), 224106.
19. Smrcok, L., Rietveld Refinement of Y2o3 Using the Pearson Vii Profile Shape Function. *Crystal Research and Technology* **1989,** *24* (6), 607-611.
20. Tomiki, T.; Tamashiro, J.; Tanahara, Y.; Yamada, A.; Fukutani, H.; Miyahara, T.; Kato, H.; Shin, S.; Ishigame, M., Optical-Spectra of Y2o3 Single-Crystals in Vuv. *Journal of the Physical Society of Japan* **1986,** *55* (12), 4543-4549.
21. Ming, W.; Chen, S.; Du, M.-H., Chemical instability leads to unusual chemical-potential-independent defect formation and diffusion in perovskite solar cell material CH3NH3PbI3. *Journal of Materials Chemistry A* **2016,** *4* (43), 16975-16981.
22. Lany, S.; Zunger, A., Assessment of correction methods for the band-gap problem and for finite-size effects in supercell defect calculations: Case studies for ZnO and GaAs. *Physical Review B* **2008,** *78* (23), 235104.
23. Mason, T.; Gonzalez, G.; Hwang, J.-H.; Kammler, D., Point defects and related properties of highly co-doped bixbyite In 2 O 3. *Physical Chemistry Chemical Physics* **2003,** *5* (11), 2183-2189.
24. Chase, M. W.; Davies, C. A.; Downey, J. R.; Frurip, D. J.; Mcdonald, R. A.; Syverud, A. N., Janaf Thermochemical Tables - 3rd Edition .2. *Journal of Physical and Chemical Reference Data* **1985,** *14*, 927-1856.
25. Reuter, K.; Scheffler, M., Composition, structure, and stability of ${\mathrm{RuO}}_{2}(110)$ as a function of oxygen pressure. *Physical Review B* **2001,** *65* (3), 035406.
26. Shionoya, S.; Yen, W. M.; Yamamoto, H., *Phosphor handbook*. CRC press: 2006.